Supplement of Geosci. Model Dev., 17, 5123–5144, 2024
https://doi.org/10.5194/gmd-17-5123-2024-supplement

Geoscientific Model Development
Open Access

Supplement of

Coupling a large-scale glacier and hydrological model (OGGM v1.5.3 and CWatM V1.08) – towards an improved representation of mountain water resources in global assessments

Sarah Hanus et al.

Correspondence to: Sarah Hanus (sarah.hanus@geo.uzh.ch)

Supplementary Materials

List of Figures

List of Tables

S1 Model Coupling Approach

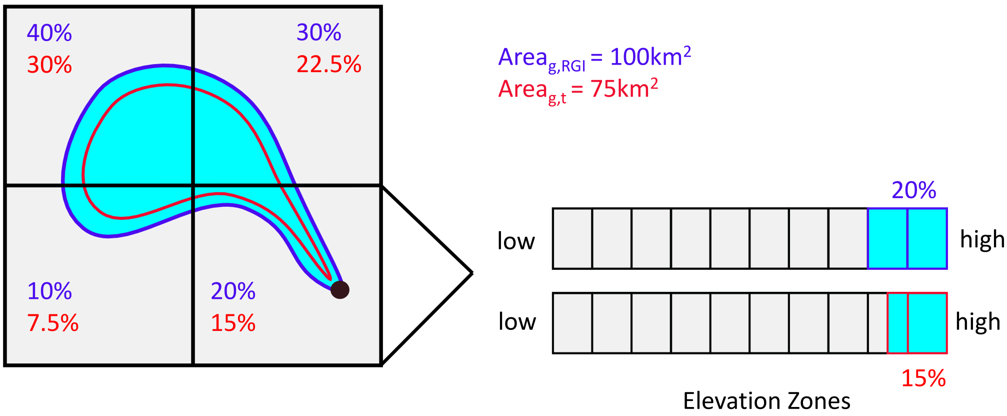

Figure S1: Schematization of the area reduction approach for a glacier that covers multiple grid cells used in this study. The same relative area reduction is applied to all grid cells that the glacier covers. In each grid cell, the glacier covered area is omitted in CWatM as shown on the right hand side. The black dot on the left hand side indicates the terminus of the glacier and therefore the grid cell to which glacier-sourced melt of the entire glacier is routed.

S2 Model Evaluation

S2.1 Snow cover penalty

The penalty for the snow cover error is a simple function that ensures that the automatic calibration is not steered to parameter sets that represent the discharge well at the cost of snow cover representation. Therefore, we assumed the mean snow cover in the selected river basins should be close to zero for at least two months per year. To build a penalty sensitive to snow accumulation, we set a threshold of 0.2m above which the objective function is negative (Eq. S1). We combine the snow cover error penality with the non-parametric KGE to obtain a single objective function for calibration (Eq. S2).

$$O_{SC} = 1 - (S_{mean,2months}/0.2) \tag{S1}$$

$$O_{tot} = 0.8 \cdot O_{KGE} + 0.2 \cdot O_{SC} \tag{S2}$$

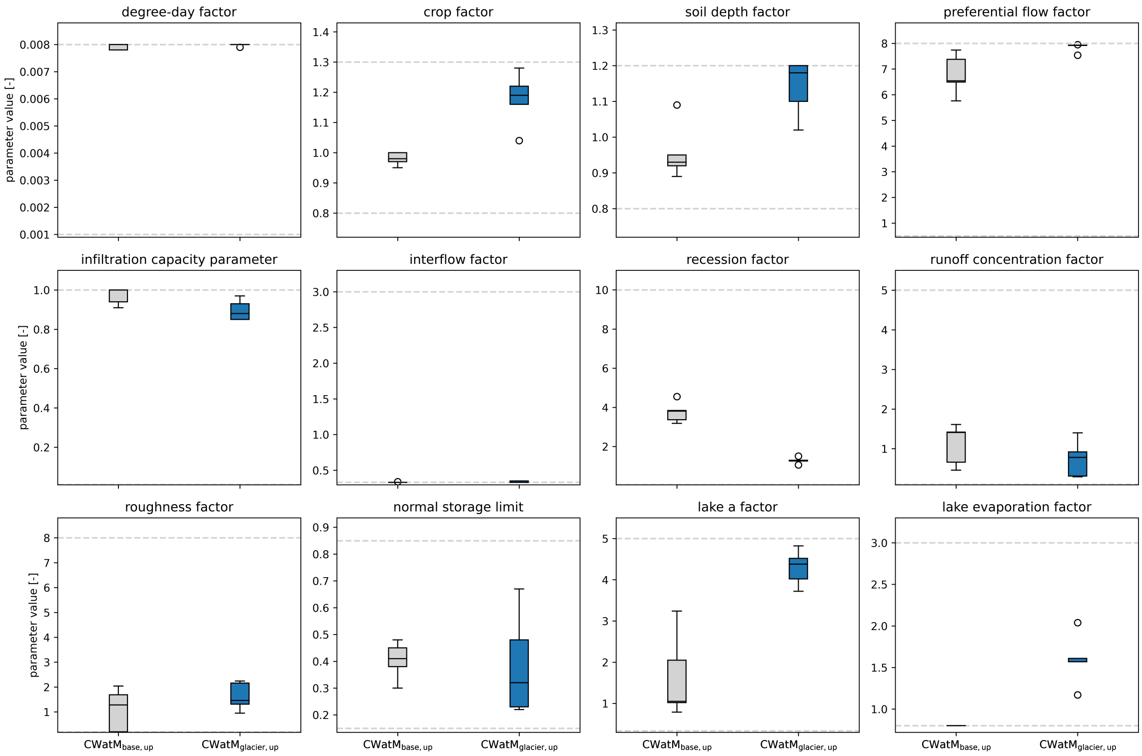

Figure S2: Comparison of the parameter values of $\mathrm{CWatM_{base}}$ and $\mathrm{CWatM_{glacier}}$ for the upstream station of the Rhone river basin. Each boxplot comprises five parameter values. The dashed lines depict the parameter range. The parameters are explained in Burek et al. (2020) (Table 2). The crop factor, the preferential flow factor, the lake evaporation factor and the soil depth factors are lower for $\mathrm{CWatM_{base}}$ than for $\mathrm{CWatM_{glacier}}$, whereas the recession factor is higher. This reduces evapotranspiration in $\mathrm{CWatM_{base}}$ to compensate for missing glacier runoff.

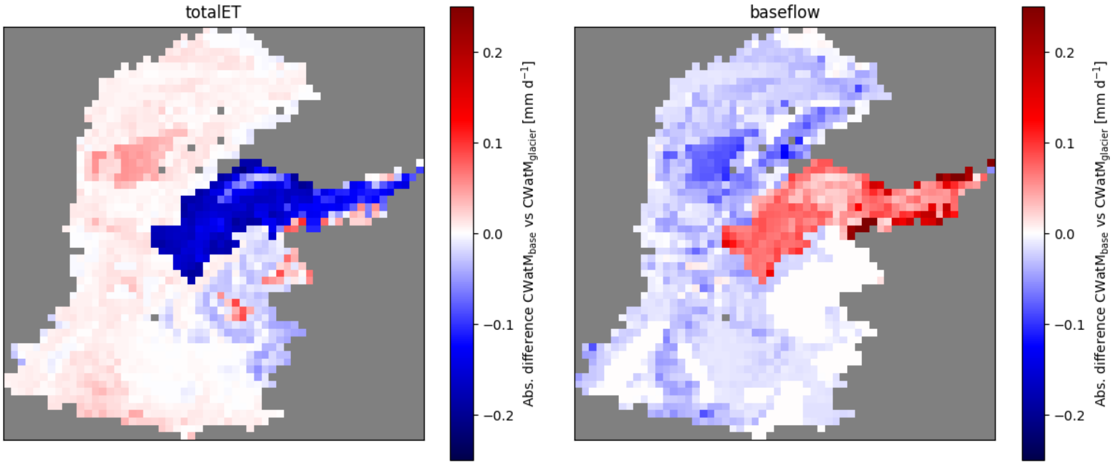

Figure S3: Spatial comparison of mean total evapotranspiration and groundwater contributions to streamflow (baseflow) in the Rhone river basin. The variables over the five parameter sets for each $\mathrm{CWatM_{base}}$ and $\mathrm{CWatM_{glacier}}$ are compared. The difference in parameter sets upstream leads to lower evapotranspiration and higher baseflow in $\mathrm{CWatM_{base}}$. Only in upstream grid cells with glacier cover, the evapotranspiration in $\mathrm{CWatM_{base}}$ is higher because OGGM assumes no evapotranspiration on glaciers.

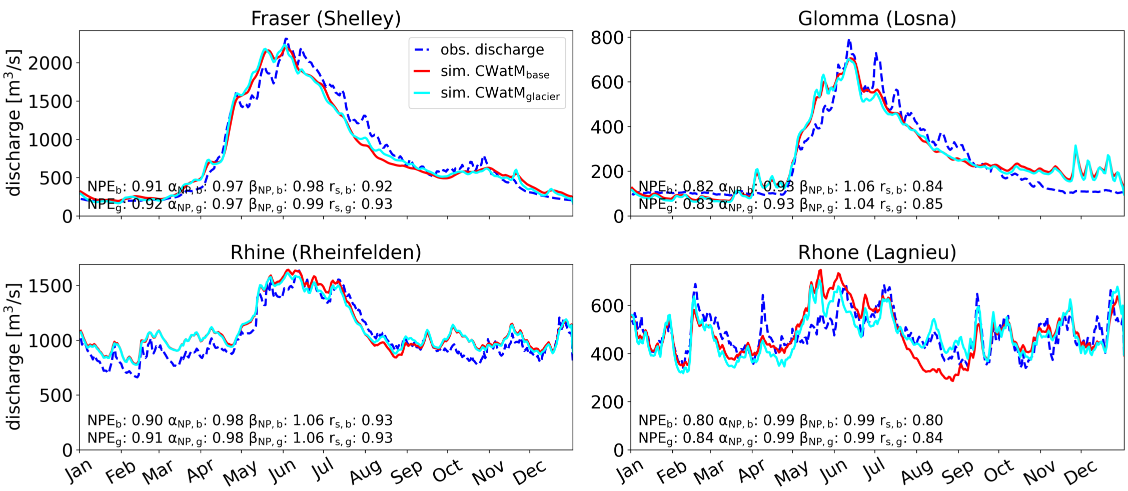

Figure S4: Mean hydrographs of the evaluation period (1990–1999) for the upstream station of the study basins. As insert the NPE and its error components over the whole evaluation period are given for $\mathrm{CWatM_{base}}$ (index b) and $\mathrm{CWatM_{glacier}}$ (index g) (α_{NP}: variability, β_{NP}: mean, r_s: dynamics; Pool et al., 2018). Values closer to 1 indicate a better match.

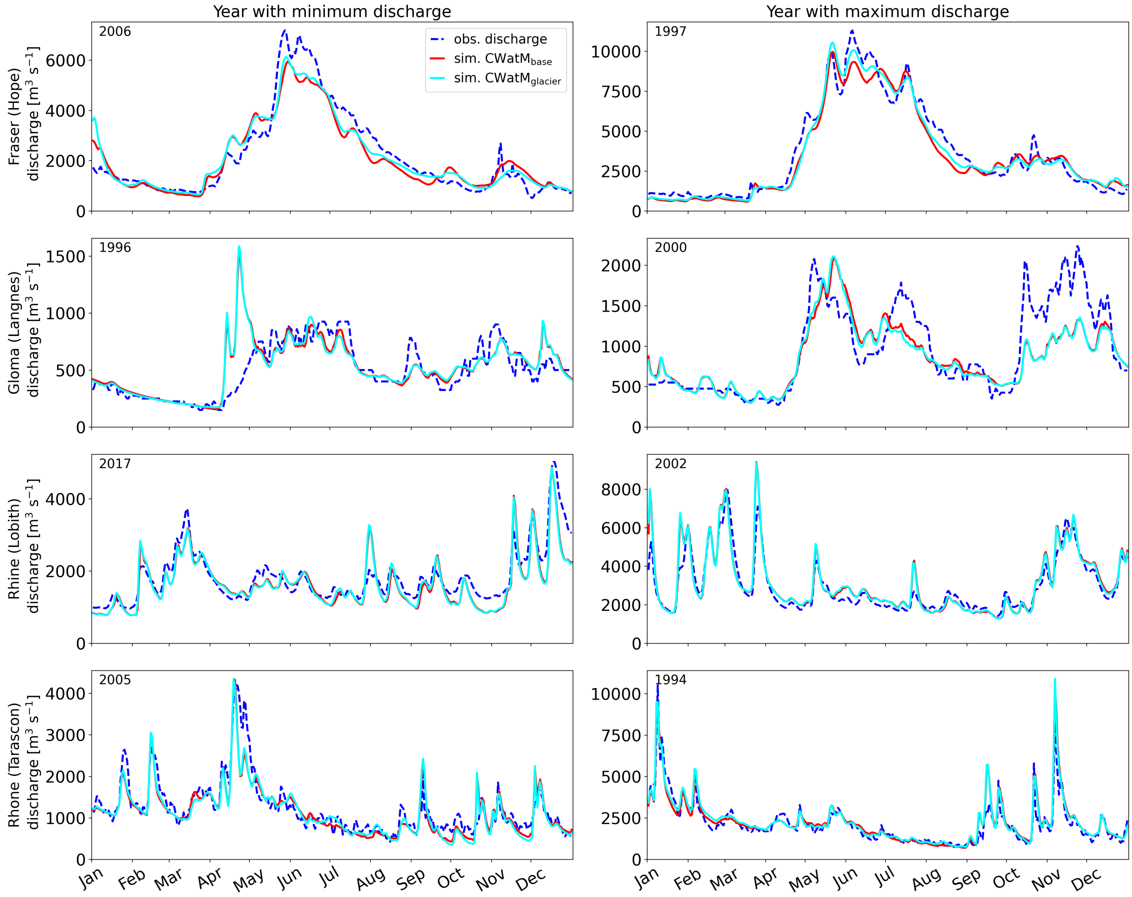

Figure S5: Hydrographs of the year with minimum and maximum annual discharge sum during the 30-year period 1990–2019 for the downstream stations of the study basins. Years 2000 or later fall within the calibration period. For the Rhone, the year with the second smallest discharge was chosen as the minimum year, because for the year with the lowest discharge, no observational data was available.

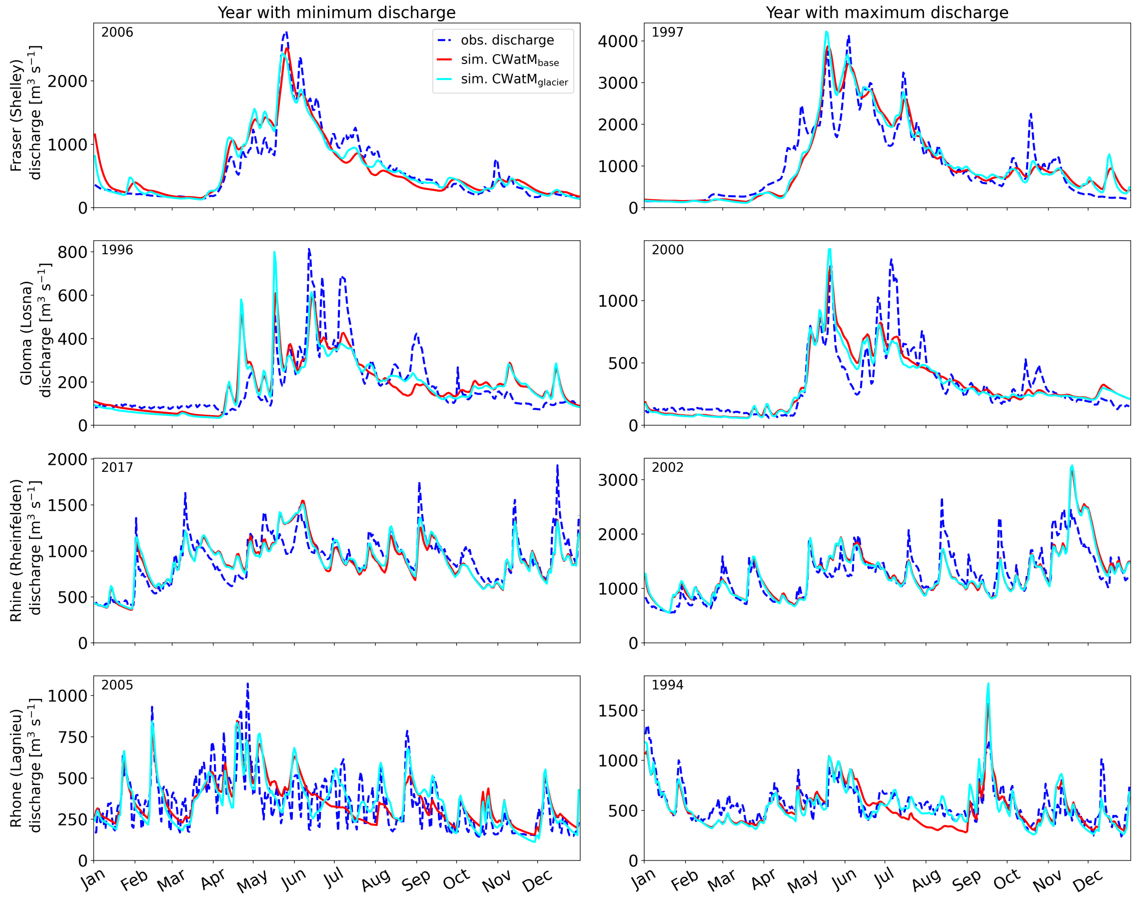

Figure S6: Hydrographs of the year with minimum and maximum annual discharge sum for the upstream stations of the study basins. For the Rhone, the year with the second smallest discharge was chosen as the minimum year, because for the year with the lowest discharge, no observational data was available.

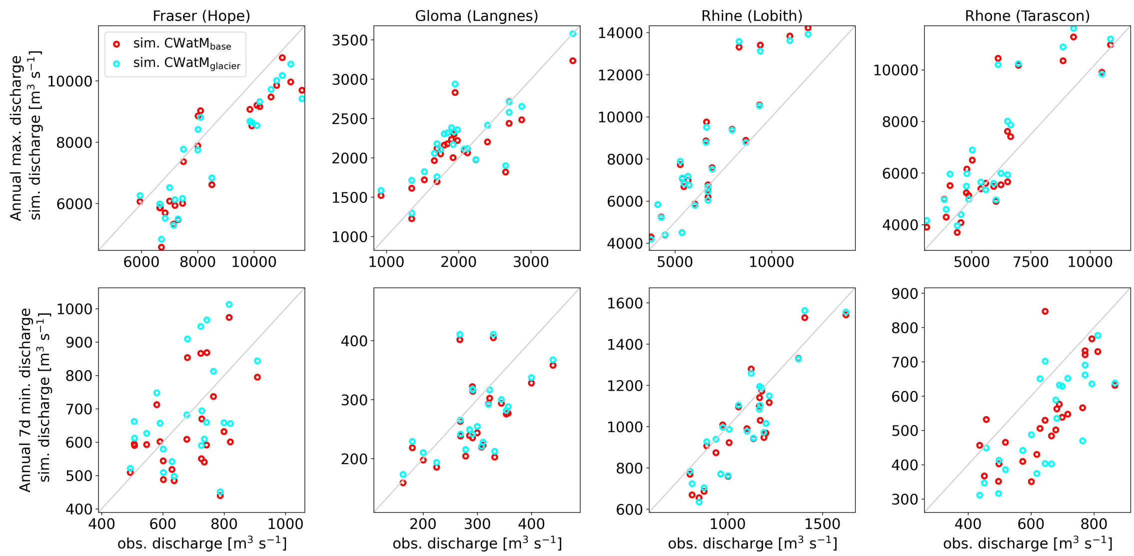

Figure S7: Simulated against observed annual minimum and maximum discharge of the 30 years in the past (1990–2019). The different colours refer to CWatM$_{\text{base}}$ and CWatM$_{\text{glacier}}$.

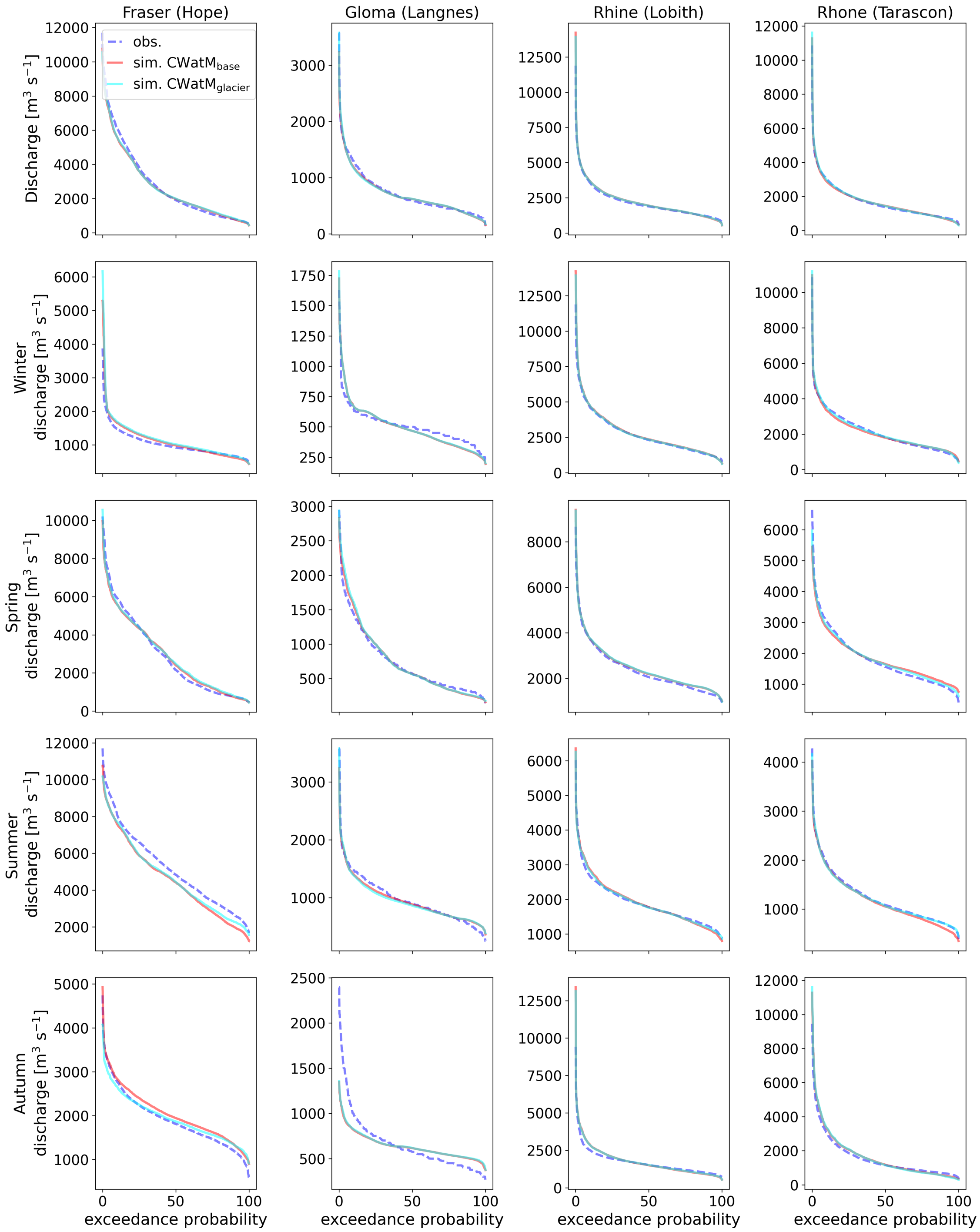

Figure S8: Comparison of flow duration curves of discharge data from 1990 until the last year of available observations (Fraser: 2016, Gloma and Rhine: 2018, Rhone: 2014). Over the whole period (first row) and split by seasons (Winter:Dec-Feb, Spring:Mar-May, Summer:Jun-Aug, Autumn:Sep-Nov)

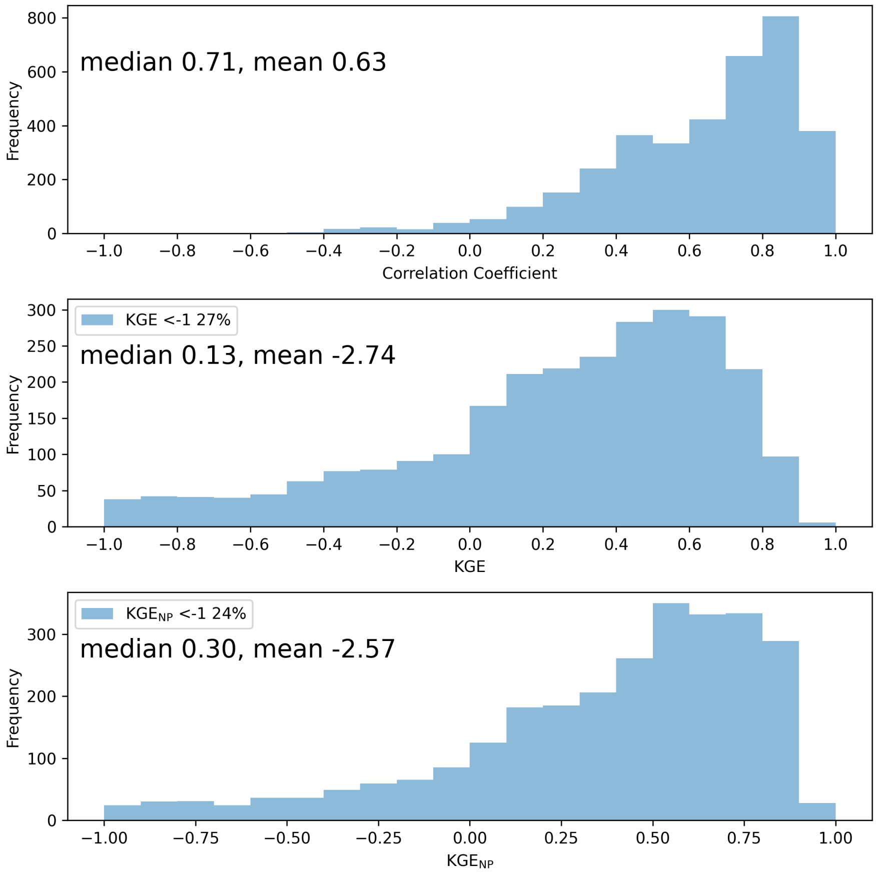

Figure S9: Histograms of performance of six global parameter sets: Correlation coefficient, KGE and the non-parametric version of the KGE (KGE_{NP}) of monthly discharge. The mean and median values are annotated as well as the percentage of gauges with KGE and KGE_{NP} below -1.

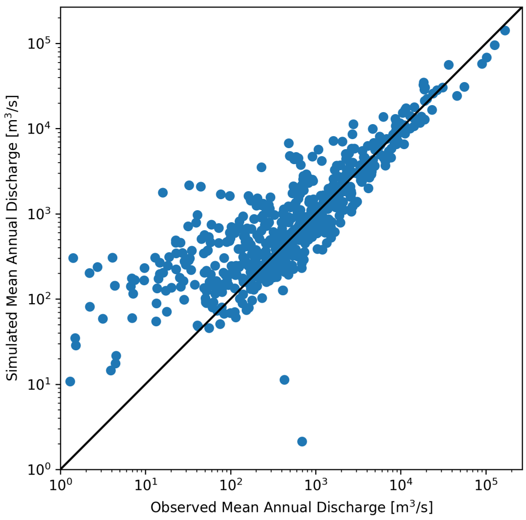

Figure S10: Simulated compared to observed mean annual discharge at gauges used for calibration for the time period 1990–2019. The ensemble mean of simulations with six parameter sets is used.

S3 Future changes in study basins (5 arcmin)

S3.1 Estimating median temperature increase compared to pre-industrial levels

For estimating median temperature increases of 2070–2099 compared to the pre-industrial era, we used the estimates of past temperature increases from the IPCC AR6 report (Figure 1.12 IPCC, 2021). This shows that the temperature increase in the period 1986–2005 was 0.69°C and in 1995-2014 0.85°C compared to pre-industrial levels. We thus calculated the global mean temperature for the same periods with our meteorological data and the median global temperature of all GCMs for the period 2070–2099. We then derived the median temperature increase compared to pre-industrial levels. This was 1.96°C for SSP1-2.6 and 4.25°C for SSP5-8.5 for using the period 1986–2005, and 1.98°C and 4.26°C using the period 1995–2014, respectively. Thus, we rounded the temperature increase in our manuscript to 2.0°C and 4.3°C.

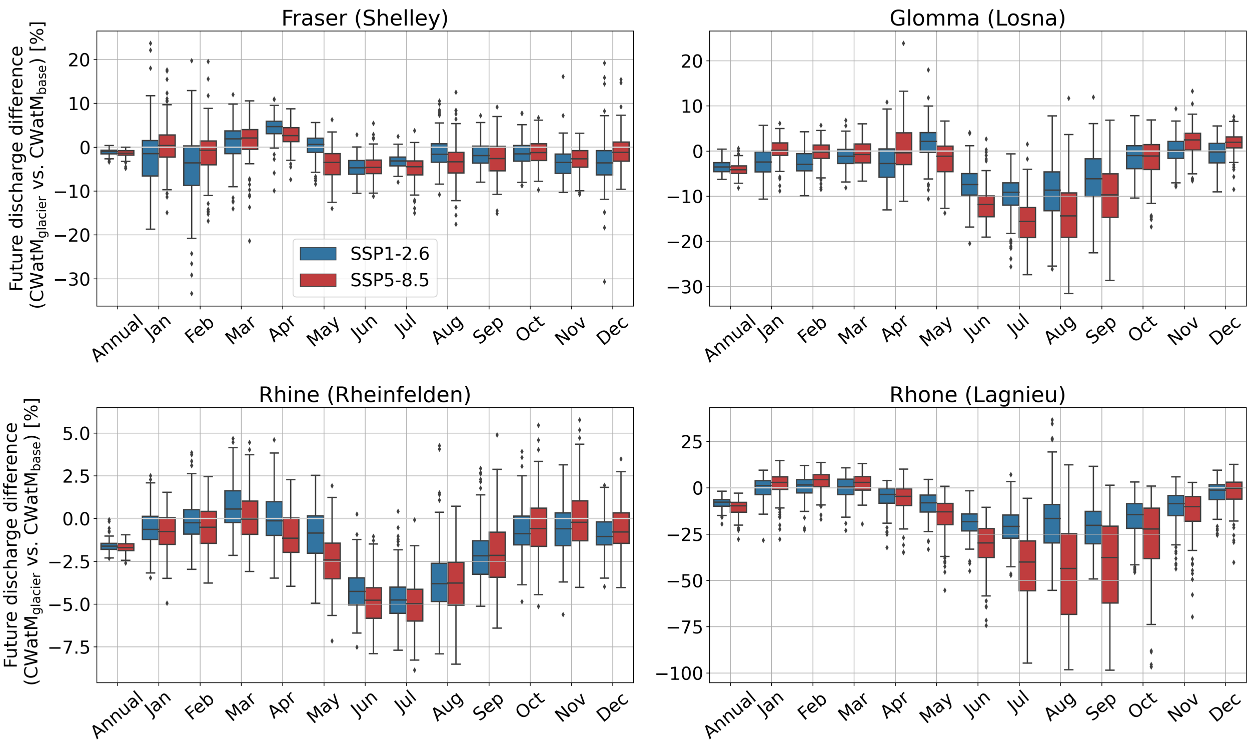

Figure S11: Relative difference in mean annual and mean monthly discharge of $CWatM_{glacier}$ compared to $CWatM_{base}$ at the upstream gauges for 30 years from 2070–2099, shown per SSP scenario which translate into warming levels of +1.9°C and +4.2°C compared to pre-industrial time.

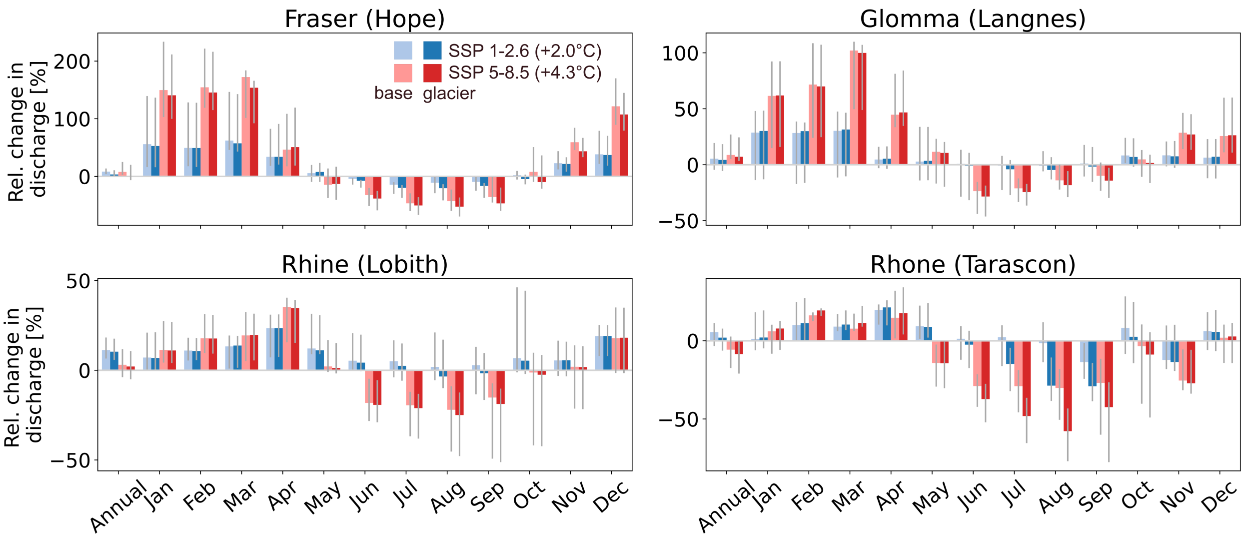

Figure S12: Relative change in mean annual and mean monthly discharge at the downstream stations for the period 2070–2099 compared to 1990–2019 for $\mathrm{CWatM_{base}}$ and $\mathrm{CWatM_{glacier}}$, shown per SSP scenario which translate into warming levels of +1.9°C and +4.2°C compared to pre-industrial time. The height of the bar indicates median change of GCMs and the grey lines indicate the maximum and minimum change of GCMs.

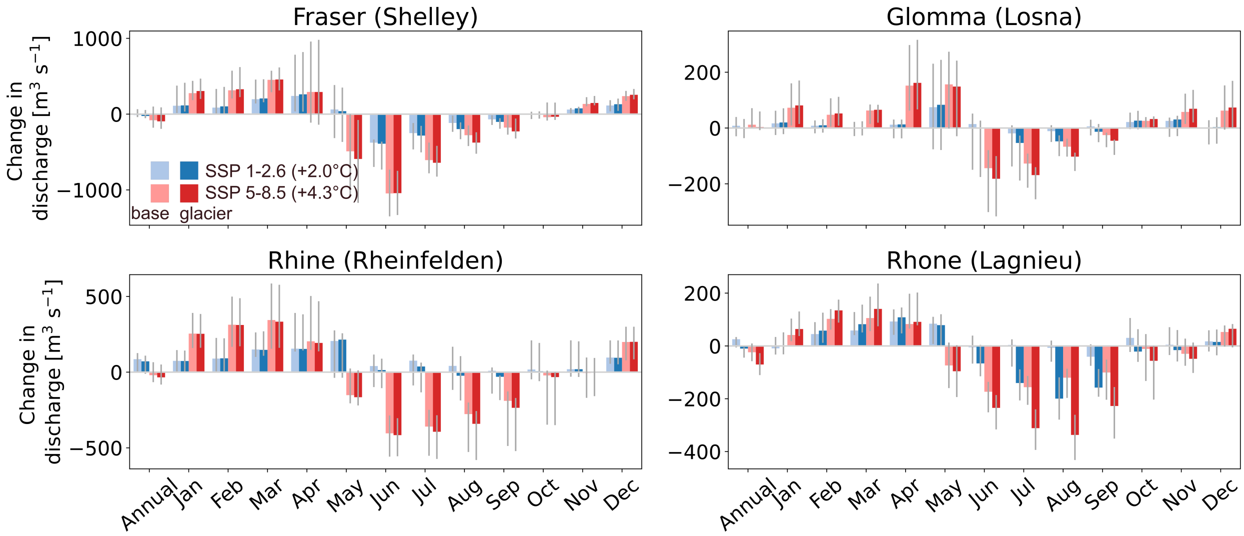

Figure S13: Absolute change in mean annual and mean monthly discharge at the upstream stations for the period 2070–2099 compared to 1990–2019 for $\mathrm{CWatM_{base}}$ and $\mathrm{CWatM_{glacier}}$, shown per SSP scenario which translate into warming levels of +1.9°C and +4.2°C compared to pre-industrial time. The height of the bar indicates median change of GCMs and the grey lines indicate the maximum and minimum change of GCMs.

S4 Changes in glacier volume, melt and glacier contribution to runoff

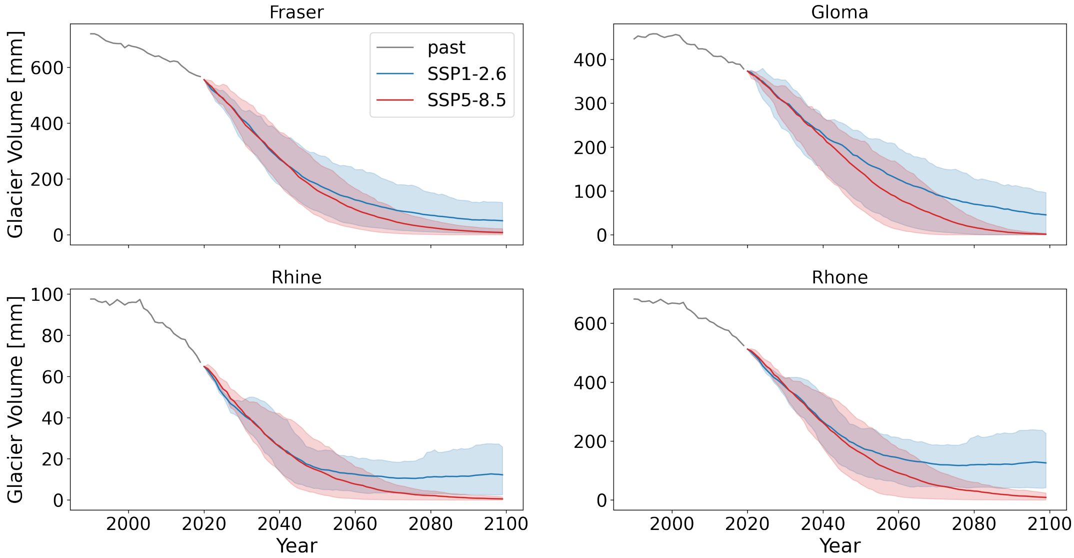

Figure S14: Glacier volumes for the selected rivers simulated with OGGM, shown as water equivalent per total river basin area [mm], per SSP scenario which translate into mean warming levels of +1.9°C and +4.2°C compared to pre-industrial time. Shaded area shows the total range of the five GCMs.

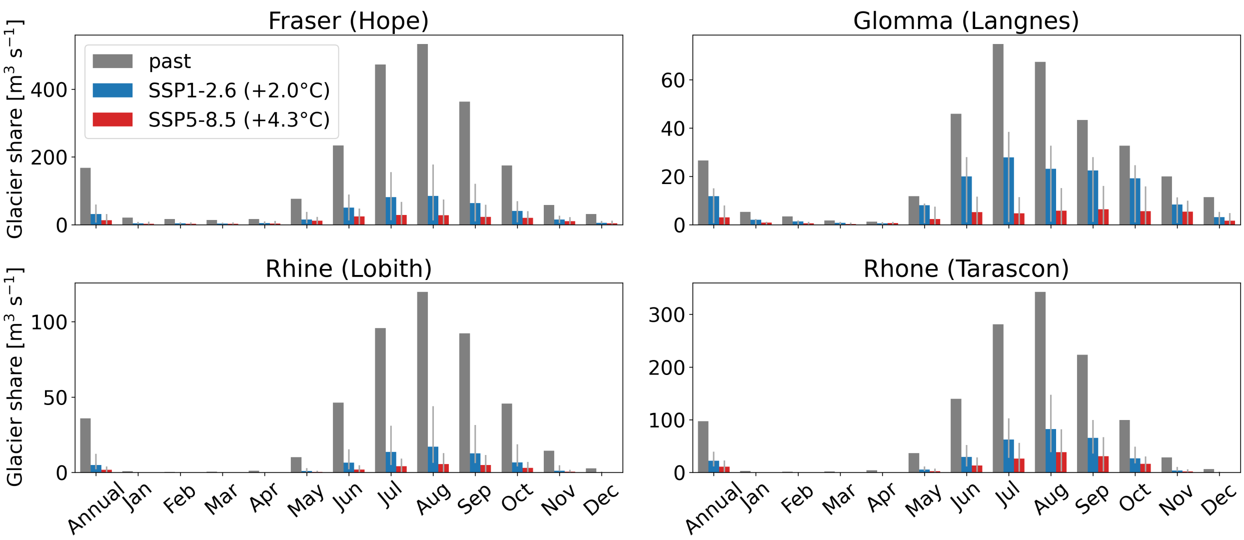

Figure S15: Absolute mean glacier contribution to annual and monthly discharge at the downstream gauge for the period 1990–2019 and for the period 2070–2099 for two SSP scenarios which translate into warming levels of +1.9°C and +4.2°C compared to pre-industrial time. The height of the bar indicates median change of GCMs and the grey lines indicate the maximum and minimum change of GCMs. Glacier contribution is estimated by subtracting $\mathrm{CWatM}_{\mathrm{glacier,bare}}$ from $\mathrm{CWatM}_{\mathrm{glacier}}$.

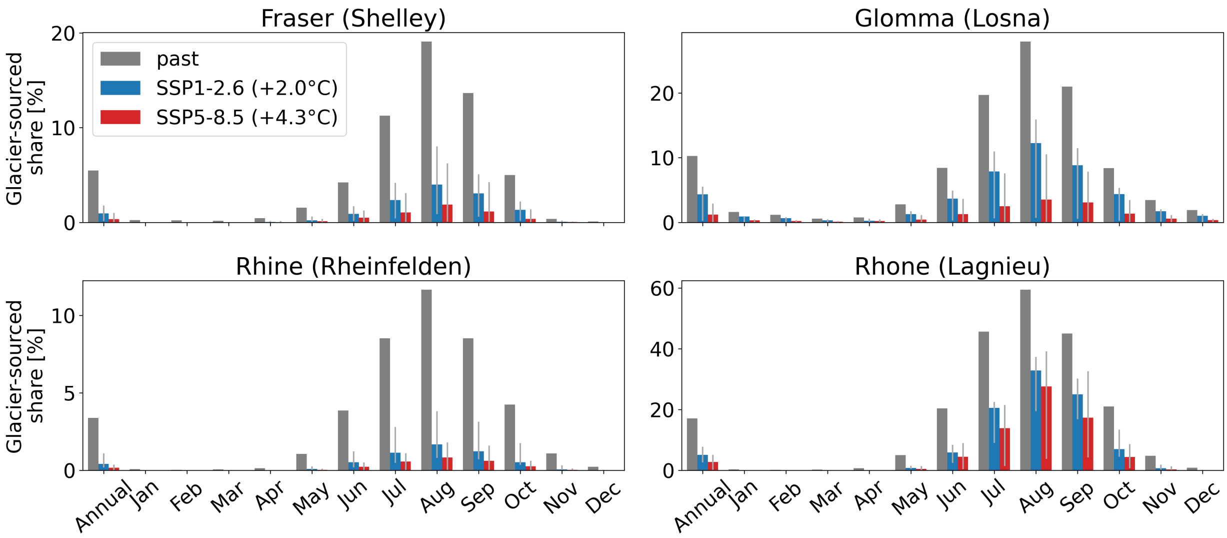

Figure S16: Relative mean glacier contribution to annual and monthly discharge at the upstream gauge for the period 1990–2019 and for the period 2070–2099 for two SSP scenarios which translate into warming levels of +1.9°C and +4.2°C compared to pre-industrial time. The height of the bar indicates median change of GCMs and the grey lines indicate the maximum and minimum change of GCMs. Glacier contribution is estimated by subtracting $\mathrm{CWatM}_{\mathrm{glacier,bare}}$ from $\mathrm{CWatM}_{\mathrm{glacier}}$.

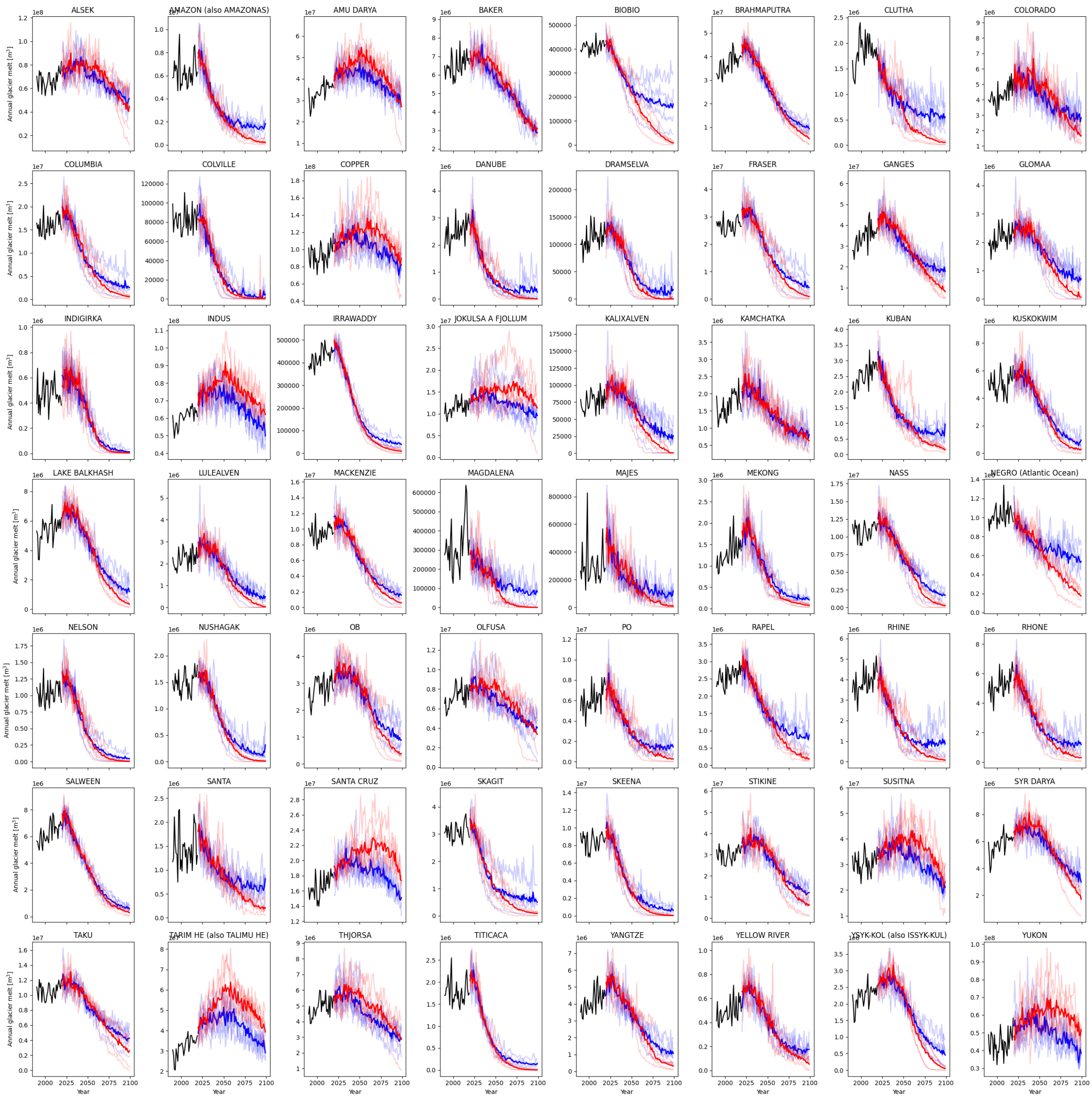

Figure S17: Simulated glacier-sourced melt volumes in the 56 glacierized river basins in the period 1990–2100. For future projections, the thick lines show multi-GCM means and thin lines denote individual GCMs results for SSP1-2.6 (blue) and SSP5-8.5 (red). Black line shows the past period (1990–2019)

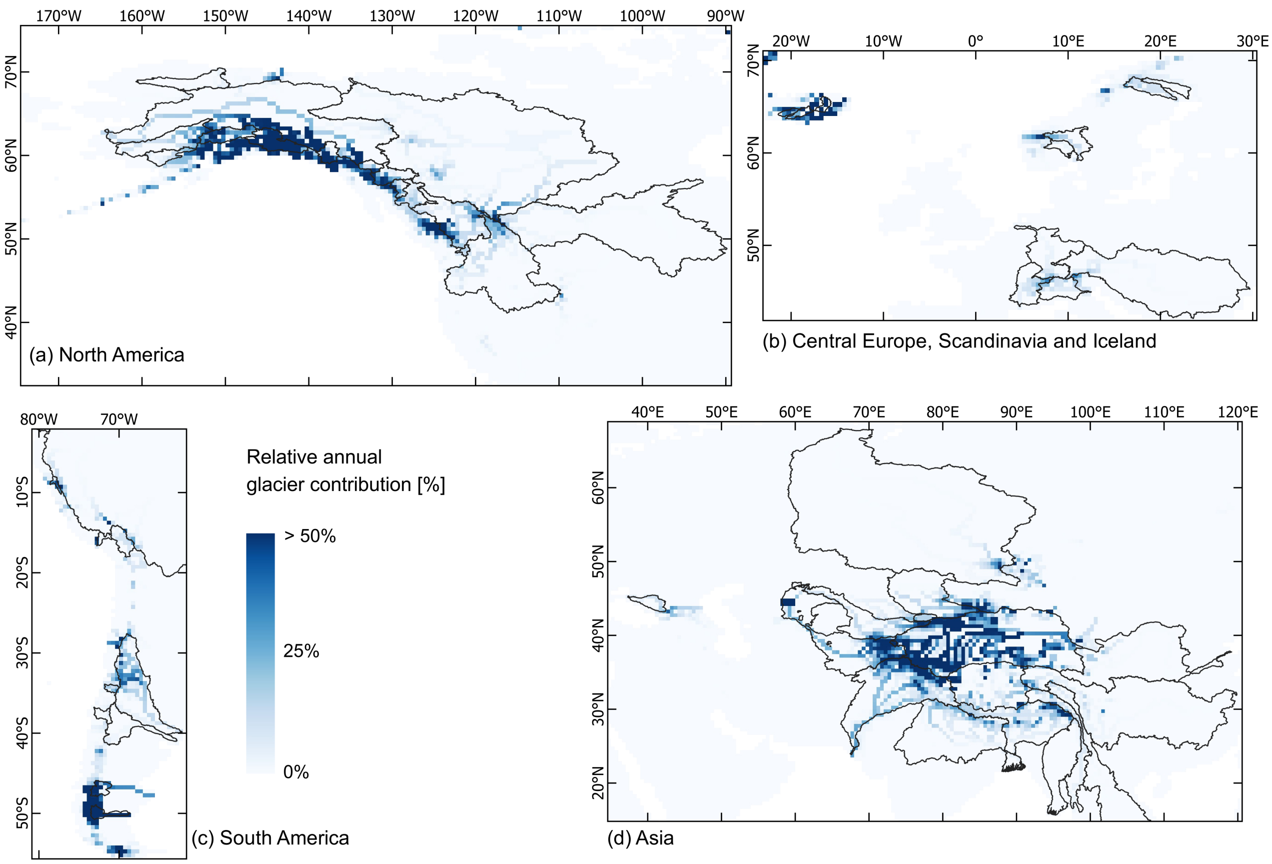

Figure S18: Relative mean glacier-sourced contribution to annual discharge for the period 1990–2019. Glacier-sourced melt comprises all melt on glaciers. Glacier contribution is estimated by subtracting $\text{CWatM}_{\text{glacier,bare}}$ from $\text{CWatM}_{\text{glacier}}$.

S5 Effects of coupling globally (30 arcmin)

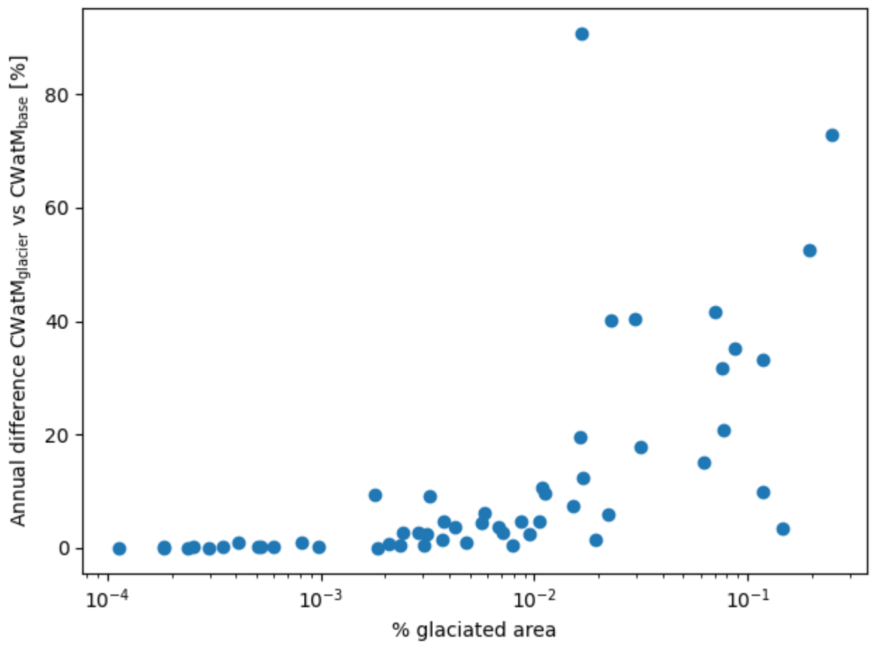

Figure S19: Relative difference in mean annual discharge between CWatM$_{glacier}$ and CWatM$_{base}$ at the outlet of 56 glacierized river basin with positive difference indicating larger discharge of CWatM$_{glacier}$ plotted against percentage of glacier area in basin. The Santa Cruz river basin is not shown here because of very high relative differences due to low discharge.

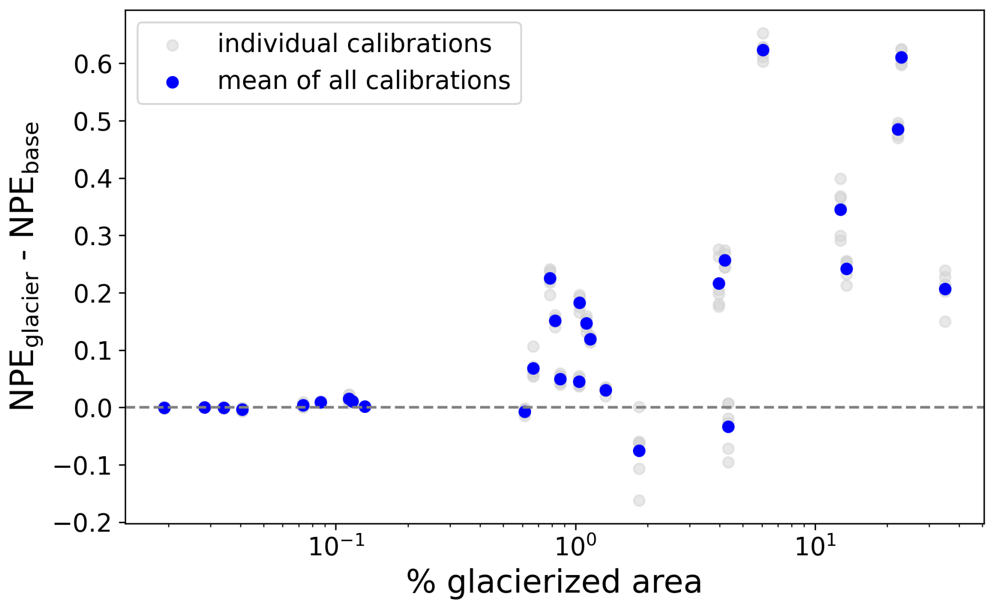

Figure S20: The performance difference between CWatM$_{glacier}$ and CWatM$_{base}$ compared to the glacier coverage. The data is the same as for Fig. 7. Results are shown for individual calibrations (grey dots) and mean of all calibrations (blue dots) for the 10 year period 2004 to 2013.

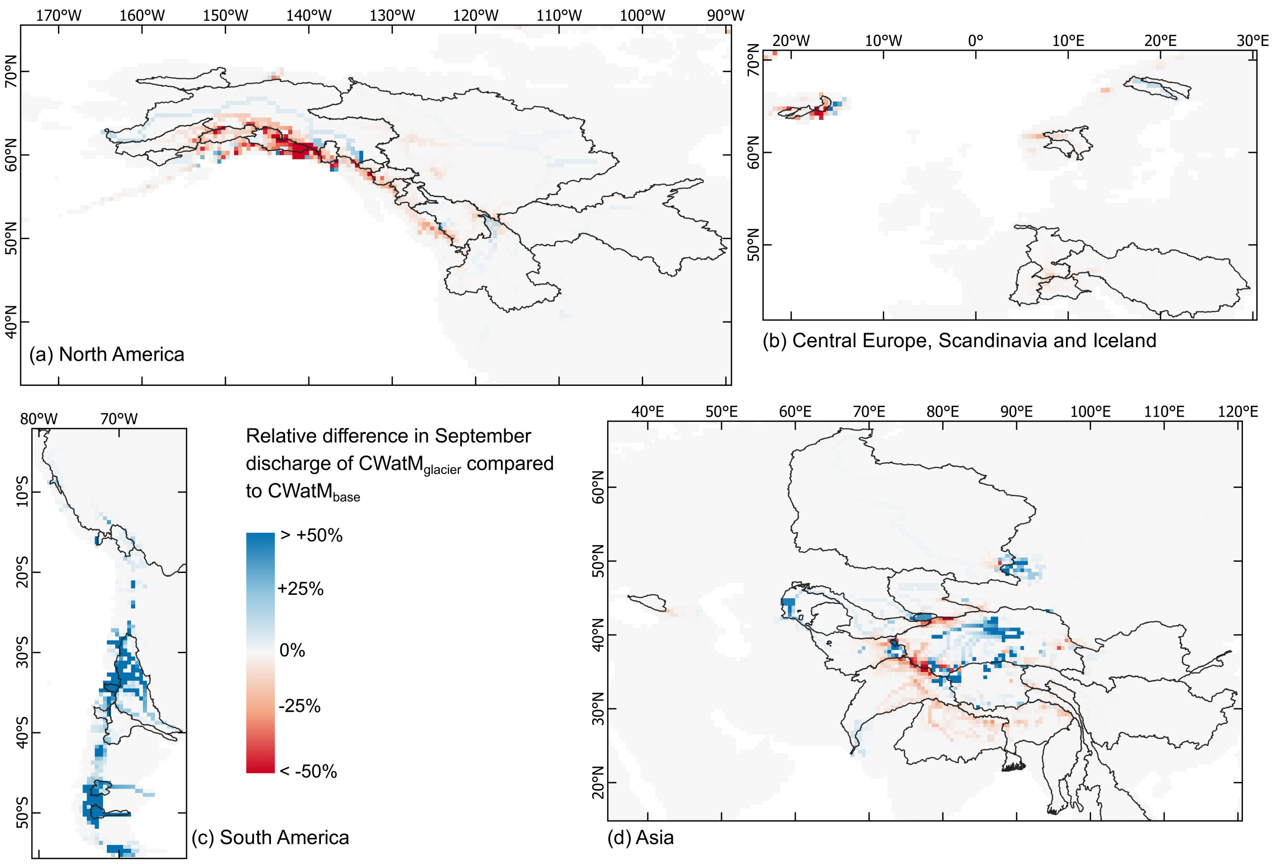

Figure S21: Relative difference in average discharge in March (1990–2019) between CWatM$_{\mathrm{glacier}}$ and CWatM$_{\mathrm{base}}$. Positive values indicate larger discharge of CWatM$_{\mathrm{glacier}}$. The major glaciated river basins are shown in black.

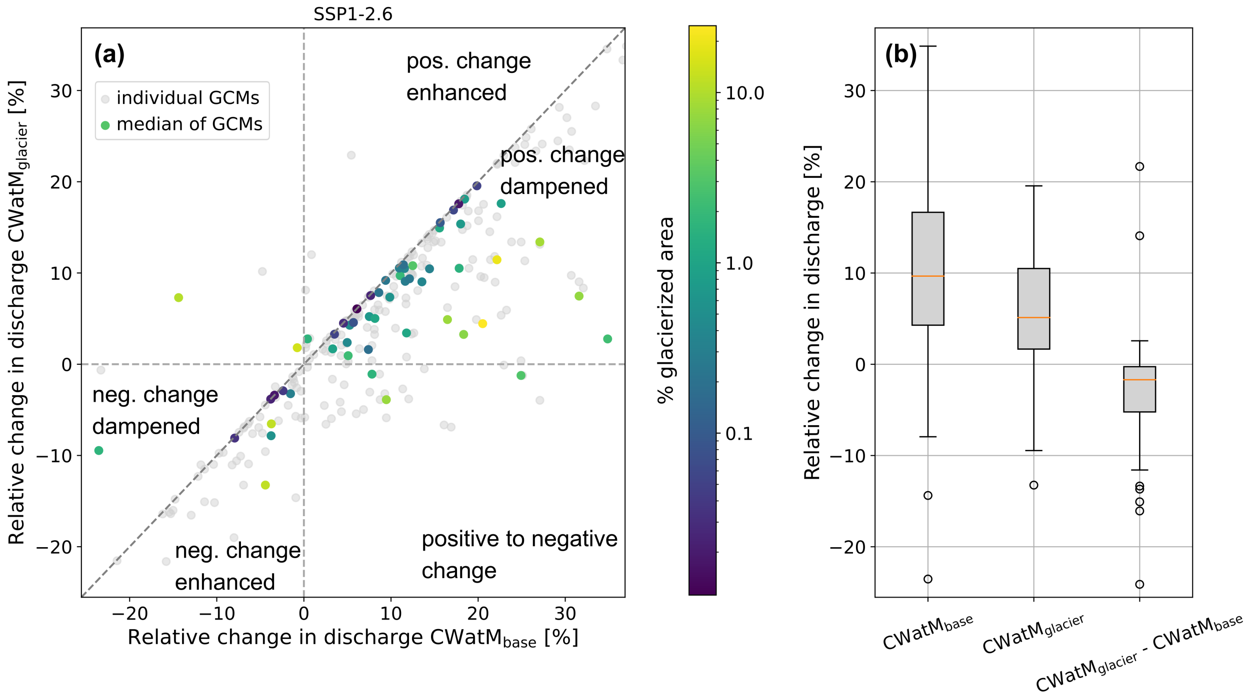

Figure S22: Comparison of relative future change for annual discharge at end of the 21st century for $CWatM_{base}$ and $CWatM_{glacier}$ for 56 glacierized river basins for SSP1-2.6. (a) Colored dots show the median of all GCMs and grey dots show individual GCMs. (b) Boxplots showing the relative future change of all basins for $CWatM_{base}$ and $CWatM_{glacier}$ and their difference.

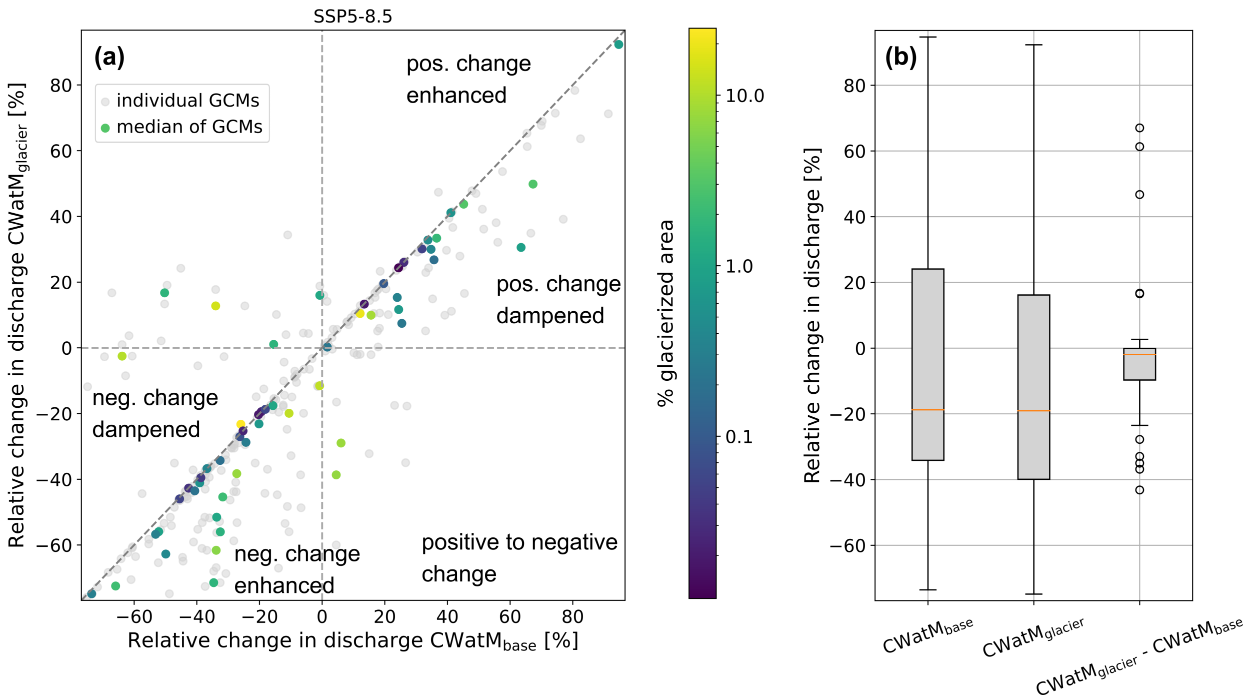

Figure S23: Comparison of relative future discharge change for the month with largest glacier-sourced melt contribution in the past at end of the 21st century for $CWatM_{base}$ and $CWatM_{glacier}$ for 56 glacierized river basins for SSP5-8.5. (a) Colored dots show the median of all GCMs and grey dots show individual GCMs. (b) Boxplots showing the relative future change of all basins for $CWatM_{base}$ and $CWatM_{glacier}$ and their difference.

S6 Influence of Precipitation Factor

The precipitation correction is handled differently in OGGM and CWatM as explained in Section 2.3 of the main paper. This difference in precipitation correction between OGGM and CWatM led to a larger precipitation input for $\text{CWatM}_{\text{glacier}}$ compared to $\text{CWatM}_{\text{base}}$ as discussed in Section 6.2.1.

The additional snowfall (S_{add}) on glaciers resulting from a precipitation factor larger than one is obtained from OGGM model output (snowfall_on, S). Snowfall on glaciers was post-processed similar to melt and rain on glaciers to obtain results per grid cells.

$$S_{add} = S/p_f \cdot (p_f - 1) \tag{S3}$$

The difference in precipitation input was assessed by comparing the precipitation/snowfall of $\text{CWatM}_{\text{base}}$ (P_{base}) to the sum of precipitation input of $\text{CWatM}_{\text{base}}$ and additional snowfall on the glaciers (S_{add}).

The precipitation input was summed across each of the 56 glacierized river basins using zonal statistics. It was repeated for a precipitation factor of $p_f = 1$, $p_f = 2$ and $p_f = 3$ (Fig. S24). Differences between $\text{CWatM}_{\text{glacier},\ p_f = 1}$ and $\text{CWatM}_{\text{base}}$ are marginal for most basins, suggesting that the impact of differences in mountainous terrain representations in the two models (discussed in Section 6.2.3) is low in most basins. Precipitation input differences between $\text{CWatM}_{\text{glacier}}$ and $\text{CWatM}_{\text{base}}$ increase with increasing p_f and are larger for snowfall. The mean difference over all basins was +5% for total precipitation and +17% for snowfall for the past period for $p_f = 3$. This shows that the difference at basin level is much lower than the difference at glacier locations, for which the snowfall input in OGGM is three times as high as in CWatM.

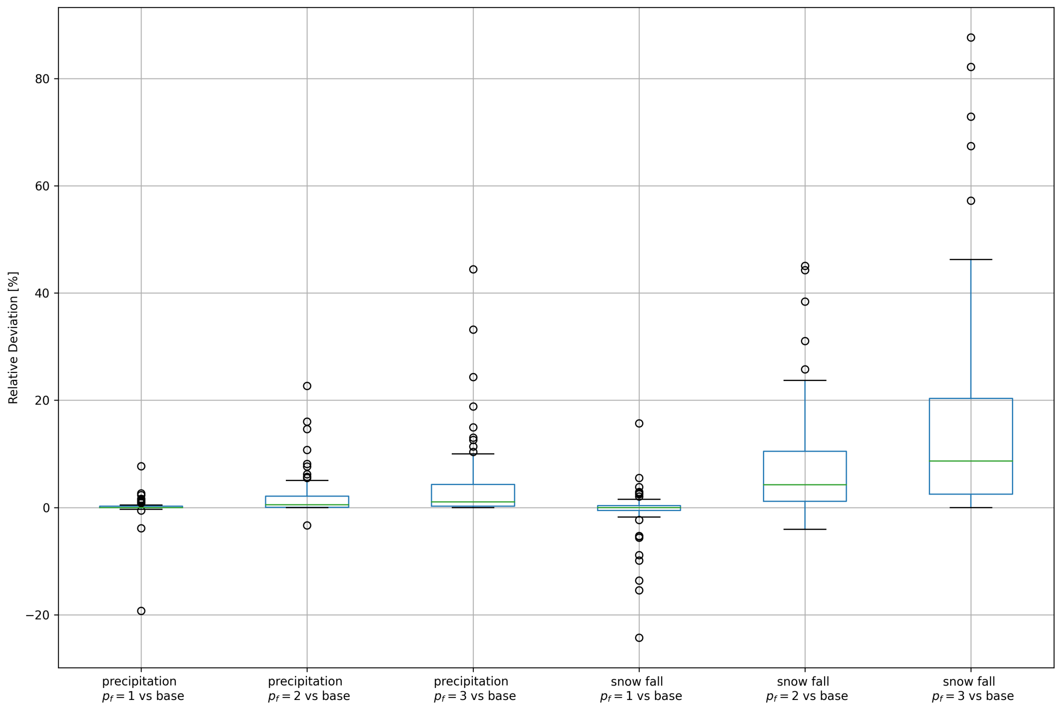

Figure S24: Boxplots of difference in precipitation and snowfall input across the 56 glacierized river basins between $\text{CWatM}_{\text{glacier}}$ with different precipitation factors (p_f) and $\text{CWatM}_{\text{base}}$ (base) for annual averages for the period 1990–2019. Each boxplot is based on 56 data points.

We also ran additional simulations with $\text{CWatM}_{\text{base}}$ using $P_{base} + S_{add}$ as input to investigate whether the performance improvement of $\text{CWatM}_{\text{glacier}}$ compared to $\text{CWatM}_{\text{base}}$ can be attributed to increased precipitation input. The results show that the performance of $\text{CWatM}_{\text{base}}$ is higher with the increased precipitation input (Fig. S25). However, this is not sufficient to explain the performance increase for $\text{CWatM}_{\text{glacier}}$ (Fig. S26). This reaffirms that including glaciers in CWatM improves its performance.

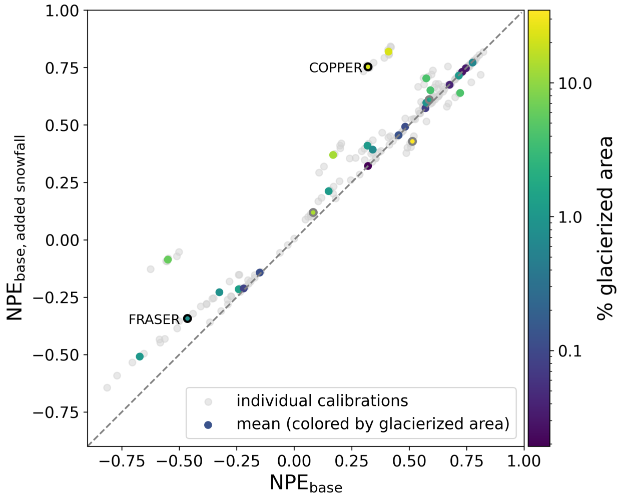

Figure S25: Performance comparison using same discharge stations as presented in Wiersma et al. (2022) between CWatM$_{\mathrm{base}}$ and CWatM$_{\mathrm{base}}$ with increased precipitation input ($P_{base} + S_{add}$) for individual calibrations (grey dots) and mean of all calibrations (coloured dots) for the 10 year period 2004 to 2013. The performance metric used is NPE (Pool et al., 2018). The Santa Cruz River basin lies outside the figure boundaries. Dots with grey outlines show basins smaller than 10,000 km^2.

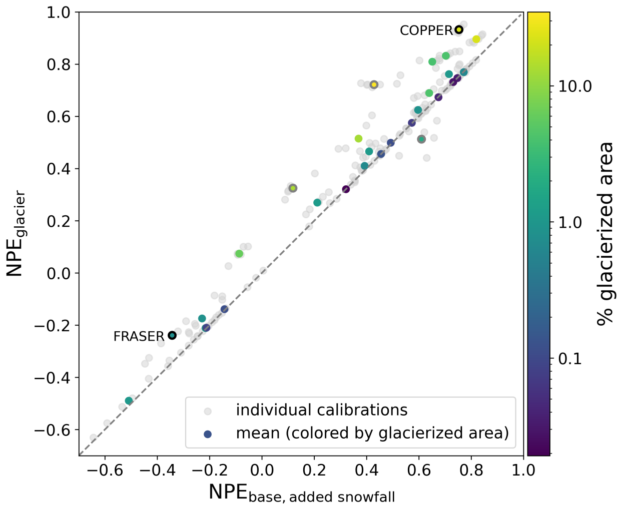

Figure S26: Performance comparison using same discharge stations as presented in Wiersma et al. (2022) between CWatM$_{\mathrm{base}}$ with increased precipitation input ($P_{base} + S_{add}$) and CWatM$_{\mathrm{glacier}}$ for individual calibrations (grey dots) and mean of all calibrations (coloured dots) for the 10 year period 2004 to 2013. The performance metric used is NPE (Pool et al., 2018). The Santa Cruz River basin lies outside the figure boundaries. Dots with grey outlines show basins smaller than 10,000 km^2.

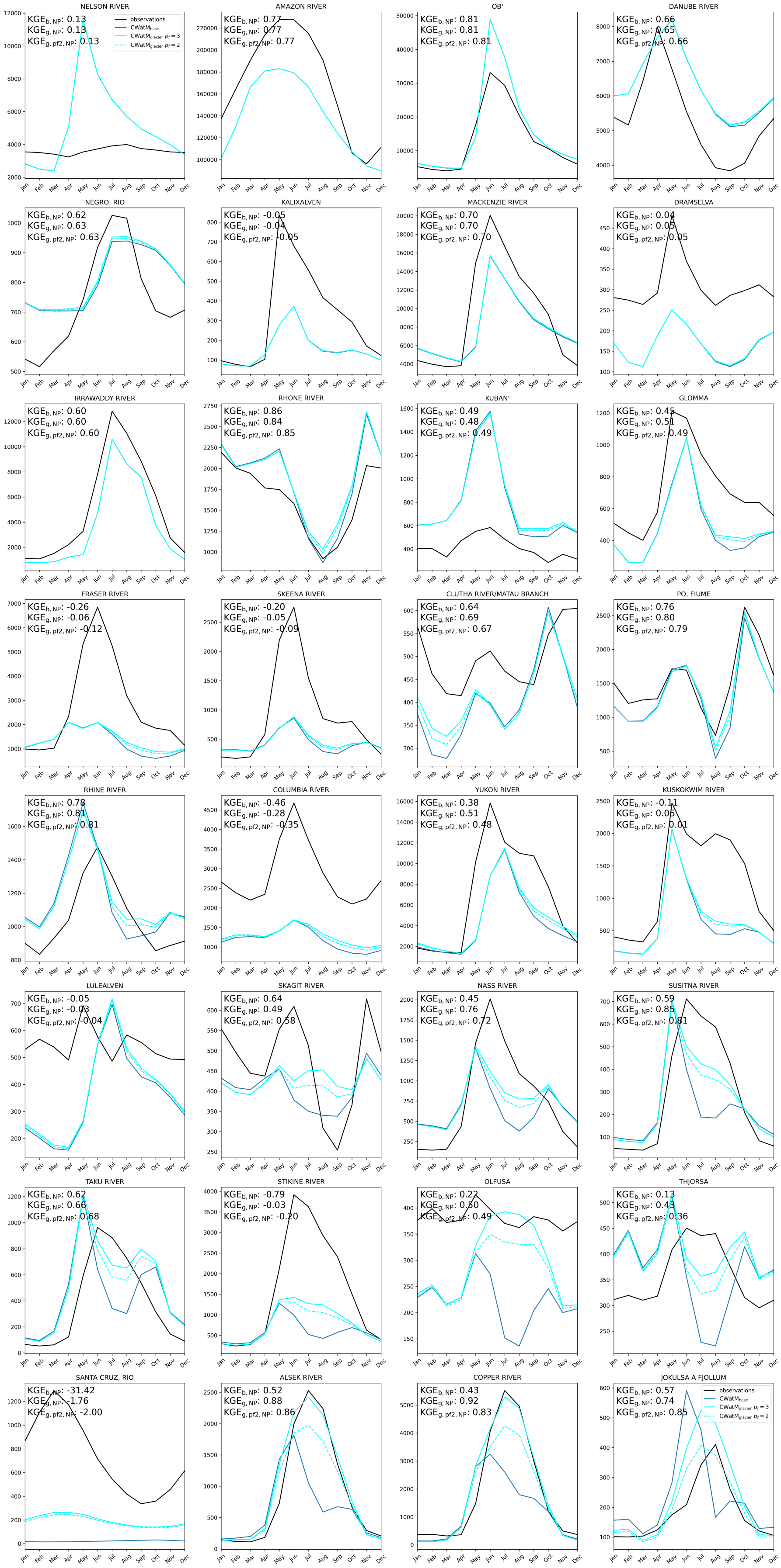

Figure S27: Comparison of mean monthly discharge between 1990–2019 of observations and simulations by $\text{CWatM}_{\text{base}}$ and $\text{CWatM}_{\text{glacier}}$ using the global parameter set used in ISIMIP3 simulations and a globally fixed precipitation factor of 2 and 3 to show the effect on hydrological simulations.

S7 Glacier location in modelling grid

Table S1: Area of basins, glacier coverage and contributing glacier melt derived from shapefiles of upstream basin area at most downstream discharge stations at 30 arcmin, 5 arcmin and 100 m resolution for 46 basins for which data was available from Burek and Smilovic (2022). Station No. refers to the GRDC station ID. Glacier melt is derived as summed annual mean glacier runoff (1990–2019) from OGGM simulations using all glaciers with terminus inside the shapefile corresponding to the respective resolution. The last three columns show the agreement of the 30 arcmin/5 arcmin resolution with the 100 m resolution.

Station No.	River Basin	Area [km2]			Glacier area [km2]			Glacier cover [%]			No. glaciers			Glacier melt [m3/s]			$\text{Area}_{rel,100m}$		$\text{Glacier area}_{rel,100m}$		$\text{Glacier melt}_{rel,100m}$	
		30arcmin	5arcmin	100m	30arcmin	5arcmin	100m	30arcmin	5arcmin	100m	30arcmin	5arcmin	100m	30arcmin	5arcmin	100m	30arcmin	5arcmin	30arcmin	5arcmin	30arcmin	5arcmin
4105710	COPPER	61714	63211	63435	14134	13810	13962	22.9	21.85	22.01	3224	3157	3170	2837.6	3451.9	3481.5	0.973	0.996	1.012	0.989	0.815	0.992
4105060	ALSEK	31151	28641	28650	6950	5992	5995	22.31	20.92	20.92	1574	1441	1424	1282	1225.1	1256.2	1.087	1	1.159	0.999	1.021	0.975
3276800	SANTA CRUZ	15966	17113	17029	3529	3220	3098	22.1	18.82	18.19	477	490	457	302.6	289.7	294.3	0.938	1.005	1.139	1.039	1.028	0.984
4105800	SUSITNA	54380	49950	49845	4216	4355	4358	7.75	8.72	8.74	1283	1249	1272	407.8	438.7	446.7	1.091	1.002	0.967	0.999	0.913	0.982
3186500	BAKER	14926	22435	22861	1767	1710	1715	11.84	7.62	7.5	1162	1474	1524	154	262.2	267.9	0.653	0.981	1.03	0.997	0.575	0.979
4204900	STIKINE	51387	50707	50658	3113	3460	3552	6.06	6.82	7.01	2179	2241	2290	387	516.4	534.5	1.014	1.001	0.876	0.974	0.724	0.966
4245100	NASS	18982	18740	18377	753	1317	1234	3.97	7.03	6.71	796	791	741	145.2	213.9	221.5	1.033	1.02	0.61	1.067	0.656	0.966
4206601	TAKU	17655	17017	16860	765	1190	1023	4.33	7	6.07	414	616	593	143.4	327.5	285.1	1.047	1.009	0.748	1.163	0.503	1.149
2335950	INDUS	821086	834863	833842	25876	27359	27042	3.15	3.28	3.24	22384	22991	22795	706	720	725.9	0.985	1.001	0.957	1.012	0.973	0.992
3948300	SANTA	15301	11988	11951	325	363	349	2.12	3.03	2.92	399	426	405	17.2	20.5	19.1	1.28	1.003	0.931	1.04	0.901	1.076
2817100	AMU DARYA	451358	372771	372568	9695	9724	9789	2.15	2.61	2.63	11854	11564	11702	391.6	400.2	411.1	1.211	1.001	0.99	0.993	0.953	0.973
2651100	BRAHMAPUTRA	525994	514210	514170	9748	10382	10506	1.85	2.02	2.04	10994	11478	11430	428.8	461.6	475.7	1.023	1	0.928	0.988	0.901	0.97
3179250	RAPEL	12781	13485	13503	379	284	235	2.97	2.11	1.74	447	275	238	32	26.9	26.1	0.947	0.999	1.613	1.209	1.225	1.033
4103200	YUKON	816227	821514	821207	9054	10313	10356	1.11	1.26	1.26	3005	3095	3082	1138.7	1364.8	1353.9	0.994	1	0.874	0.996	0.841	1.008
4102100	KUSKOKWIM	82259	80037	80296	946	894	973	1.15	1.12	1.21	752	817	872	77.6	104.4	119.3	1.024	0.997	0.972	0.919	0.651	0.875
6233750	LULEALVEN	24134	24460	24474	322	233	263	1.33	0.95	1.08	243	233	244	27.8	20.1	28.1	0.986	0.999	1.224	0.886	0.987	0.714
6139100	RHONE	99516	94110	93590	612	891	916	0.61	0.95	0.98	1013	1195	1177	71.9	101.7	107.6	1.063	1.006	0.668	0.973	0.669	0.946
4207900	FRASER	216641	216166	216412	1694	1729	1845	0.78	0.8	0.85	1912	1937	1959	157.9	152	178.9	1.001	0.999	0.918	0.937	0.883	0.85
4245250	SKEENA	42158	41945	41861	347	366	357	0.82	0.87	0.85	608	601	586	33.5	36.7	37.6	1.007	1.002	0.972	1.025	0.892	0.978
2646100	GANGES	933315	945500	945040	7479	8007	7831	0.8	0.85	0.83	6407	6652	6559	396	445.6	455.3	0.988	1	0.955	1.022	0.87	0.979
2314450	LAKE BALKHASH	13201	13084	12970	86	122	106	0.65	0.93	0.81	126	185	179	6	8.4	9.2	1.018	1.009	0.811	1.151	0.653	0.91
5868100	CLUTHA	19705	20477	20572	113	149	149	0.58	0.73	0.73	586	534	651	20.9	32	38.9	0.958	0.995	0.758	1	0.536	0.823
6729400	GLOMAA	41482	40356	40401	277	244	270	0.67	0.6	0.67	313	272	275	24.4	24.7	27.5	1.027	0.999	1.026	0.904	0.888	0.897
2316201	SYR DARYA	291659	335047	334279	2125	1832	1868	0.73	0.55	0.56	3526	3422	3353	76	79.3	85.4	0.873	1.002	1.138	0.981	0.89	0.928
6348800	PO	74041	73027	72903	657	381	316	0.89	0.52	0.43	1139	852	752	85.1	52.7	64.3	1.016	1.002	2.079	1.206	1.323	0.82
3275750	COLORADO	279679	302102	301986	1144	1219	1277	0.41	0.4	0.42	1336	1600	1683	45.6	54.9	61	0.926	1	0.896	0.955	0.747	0.9
2902850	KAMCHATKA	52040	51567	51457	235	175	199	0.45	0.34	0.39	175	109	136	18.8	15.4	17.5	1.011	1.002	1.181	0.879	1.075	0.881
6983350	KUBAN	48666	48434	47678	299	129	177	0.62	0.27	0.37	403	214	263	33.7	18.9	23.3	1.021	1.016	1.689	0.729	1.448	0.812
4102740	NUSHAGAK	27670	25400	25287	173	88	84	0.63	0.35	0.33	207	105	105	21.8	10.7	14.3	1.094	1.004	2.06	1.048	1.525	0.747
3179500	BIOBIO	24572	24428	24221	57	74	74	0.23	0.3	0.31	125	158	129	5.4	6.8	7.2	1.014	1.009	0.77	1	0.746	0.944
4115201	COLUMBIA	663329	651226	651439	1854	1956	1928	0.28	0.3	0.3	3519	3396	3423	187.3	195.4	213	1.018	1	0.962	1.015	0.879	0.917
6435060	RHINE	161953	158891	159333	371	329	337	0.23	0.21	0.21	724	730	793	59.1	63.9	68.1	1.016	0.997	1.101	0.976	0.867	0.939
6729311	DRAMSELVA	15178	16710	16928	18	45	27	0.12	0.27	0.16	36	48	42	1.2	6.9	5.8	0.897	0.987	0.667	1.667	0.214	1.195
2181900	YANGTZE	1696096	1682196	1681512	1067	1597	1657	0.06	0.09	0.1	1241	1535	1596	47.5	72	79.8	1.009	1	0.644	0.964	0.595	0.902
4208025	MACKENZIE	1666309	1667919	1668196	1886	1430	1404	0.11	0.09	0.08	2361	2051	2049	107.8	89.5	89	0.999	1	1.343	1.019	1.211	1.006
4101500	COLVILLE	58255	58363	58146	20	34	36	0.03	0.06	0.06	76	118	117	0.9	1.6	1.6	1.002	1.004	0.556	0.944	0.594	1.001
2903981	INDIGIRKA	307204	304604	304575	124	141	145	0.04	0.05	0.05	266	287	300	5.4	6.2	6.6	1.009	1	0.855	0.972	0.816	0.95
6742900	DANUBE	783930	790272	785184	230	339	411	0.03	0.04	0.05	612	800	857	28	46.4	54.2	0.998	1.006	0.56	0.825	0.518	0.857
3275990	NEGRO	112377	111757	113494	82	49	50	0.07	0.04	0.04	119	162	204	11.5	6.5	9.4	0.99	0.985	1.64	0.98	1.222	0.683
2569002	MEKONG	667533	668603	666773	291	211	231	0.04	0.03	0.03	507	437	471	14.9	12.4	15	1.001	1.003	1.26	0.913	0.995	0.829
4213711	NELSON	1051075	1294587	1294651	202	324	376	0.02	0.03	0.03	539	570	599	11.9	28.1	32.2	0.812	1	0.537	0.862	0.371	0.874
3629001	AMAZON	4689800	4703705	4702228	1329	1396	1438	0.03	0.03	0.03	1477	1549	1572	73.4	82.2	94.3	0.997	1	0.924	0.971	0.778	0.872
2912600	OB	2471510	2491041	2491283	841	761	759	0.03	0.03	0.03	1669	1586	1584	31.5	30.3	31	0.992	1	1.108	1.003	1.019	0.978
2180800	YELLOW RIVER	722771	740732	739525	129	130	126	0.02	0.02	0.02	170	161	162	5.7	5.8	6.8	0.977	1.002	1.024	1.032	0.838	0.86
3103300	MAGDALENA	258063	259012	258506	30	50	47	0.01	0.02	0.02	13	44	29	3.6	5.3	5.2	0.998	1.002	0.638	1.064	0.695	1.019
2260700	IRRAWADDY	357330	359729	362355	99	46	48	0.03	0.01	0.01	149	136	145	5.2	2.7	3.6	0.986	0.993	2.062	0.958	1.447	0.749

References

Burek, P. and Smilovic, M.: The use of GRDC gauging stations for calibrating large-scale hydrological models, Earth Syst. Sci Data Discussions, 2022, 1–18, 10.5194/essd-2022-231, 2022.

Burek, P., Satoh, Y., Kahil, T., Tang, T., Greve, P., Smilovic, M., Guillaumot, L., Zhao, F., and Wada, Y.: Development of the Community Water Model (CWatM v1. 04)–a high-resolution hydrological model for global and regional assessment of integrated water resources management, Geosci. Model.Dev., 13, 3267–3298, 2020.

IPCC: Climate Change 2021: The Physical Science Basis. Contribution of Working Group I to the Sixth Assessment Report of the Intergovernmental Panel on Climate Change, vol. In Press, Cambridge University Press, Cambridge, United Kingdom and New York, NY, USA, 10.1017/9781009157896, 2021.

Pool, S., Vis, M., and Seibert, J.: Evaluating model performance: towards a non-parametric variant of the Kling-Gupta efficiency, Hydrol. Sci. J., 63, 1941–1953, 2018.

Wiersma, P., Aerts, J., Zekollari, H., Hrachowitz, M., Drost, N., Huss, M., Sutanudjaja, E. H., and Hut, R.: Coupling a global glacier model to a global hydrological model prevents underestimation of glacier runoff, Hydrol. Earth Syst. Sci, 26, 5971–5986, 2022.